

See discussions, stats, and author profiles for this publication at: <https://www.researchgate.net/publication/375997509>

# Dynamic Response of RC Frames Retrofitted with Friction-Damped Brace System through Shaking Table Tests

Article in Case Studies in Construction Materials · November 2023

DOI: 10.1016/j.cscm.2023.e02725

---

CITATION

1

READS

98

4 authors, including:



Muhammad Haroon

University of Notre Dame

29 PUBLICATIONS 137 CITATIONS

[SEE PROFILE](#)

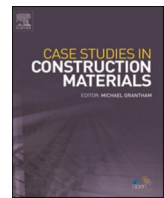


Kyung-Jae Shin

Kyungpook National University

70 PUBLICATIONS 574 CITATIONS

[SEE PROFILE](#)



## Dynamic response of RC frames retrofitted with friction-damped brace system through shaking table tests

Hye-Min Shin <sup>a</sup>, Muhammad Haroon <sup>b</sup>, Kyung-Jae Shin <sup>c</sup>, Hee-Du Lee <sup>b,\*</sup>

<sup>a</sup> Structural and Seismic Safety Research Division, Korea Atomic Energy Research Institute, Deajeon 34057, South Korea

<sup>b</sup> Regional Center for Land, Infrastructure, and Transport Technology, Kyungpook National University, Daegu 41566, South Korea

<sup>c</sup> School of Architecture, Kyungpook National University, Daegu 41566, South Korea

### ARTICLE INFO

**Keywords:**  
Seismic retrofitting  
Energy dissipation  
Friction dampers  
Shaking table test

### ABSTRACT

This study presents the shaking table test results of two-dimensional reinforced concrete (RC) frames retrofitted with a simplified friction damped brace. An easy-to-manufacture and install friction damper with economical design, was proposed and tested under reversed cyclic loading and used to retrofit RC frames. The splice of a conventional steel brace was converted into a friction damper, which not only dissipated seismic energy but also helped avoid the buckling of the steel brace. The test scheme consisted of four RC frames, and the behaviors of the three retrofitted frames were compared with that of a non-retrofitted (bare) frame. The shaking table tests were conducted using an artificial seismic wave that reflected the short-period response characteristics of the Korean earthquake. The test results of the bare and retrofitted frames were analyzed by considering several important performance indicators, such as the cracking and fracture mechanism in the RC frames, base share, and story drift ratios. The results of the shaking table tests demonstrated that the proposed damped brace effectively reduced earthquake-induced drift demands and successfully shifted the fracture and damage concentration from the columns to the beams.

### 1. Introduction

With the increasing frequency of earthquakes on the Korean Peninsula, the need for seismic retrofitting has increased for structures built prior to the introduction of modern seismic standards. Several low-to-medium-rise residential and public buildings exist in Korea with a distinct structural system in which reinforced concrete (RC) load-bearing walls at the upper stories are supported by columns on the first story with parking spaces, as shown in Fig. 1. In general, the core walls of these buildings are located far from the geometric centroid, causing plan irregularities. Such structural systems are prone to damage during earthquake events owing to soft-story mechanisms and plan irregularities. Lower-story columns have larger cross-sections and low-to-intermediate aspect ratios; therefore, they are governed by brittle shear failure. In the aftermath of the Gyeongju and Pohang earthquakes, column shear failure with limited ductility was a common failure mechanism in these buildings, as shown in Fig. 1 (right).

Over the last few decades, active research has been conducted globally to achieve optimized retrofitting schemes for structures prone to damage during earthquakes. To minimize or eliminate residual deformations in structures subjected to seismic loads, several retrofitting approaches have been investigated, such as damped-brace systems, post-tensioned tendon systems, friction and viscous

\* Corresponding author.

E-mail address: [hldza@knu.ac.kr](mailto:hldza@knu.ac.kr) (H.-D. Lee).

fluid dampers, and damped-cable systems. Rahman and Sritharan [1] and Bedoya-Rufz et al. [2] strengthened prestressed precast shear walls and RC moment frames using post-tensioned tendons. Hu et al. [3] introduced several bracing systems that increased the stiffness and restoring capacities of structures. Steel brace system is a commonly used method for retrofitting RC frames. It can increase seismic performance such as capacity, stiffness, energy dissipation, equivalent damping ratio, and ductility of structures. There are various types of connections that can be used and suggested to apply the steel brace. The steel brace system with different type of connection has been evaluated in numerous studies using both full-scale experiments and numerical analyses [4–7]. One of the common types of steel brace is X-bracing. The effects of X-bracing were evaluated through experimentation and analysis by many researchers [8,9]. Additionally, there are design proposals aimed at addressing buckling issues caused by compression. Based on previous research findings, it is essential to consider factors such as the number of stories and the strength of columns in RC frames when determining the appropriateness of brace design strength [10].

A self-centering system has been developed to reduce and prevent structural damage under severe seismic load. A shape memory alloys (SMAs) which has superelastic behavior has increasingly studied for restoring force mechanisms in several years [11–15]. Many studies have been dedicated to SMA-brace devices applied to structure frames by investigating the seismic and collapse performance of SMAs using experimental and analytical studies [16–18]. Dolce and Cardone [19] and Ingalkar [20] utilized SMA in dampers that provided high energy dissipation owing to their superelastic characteristics. Casagrande et al. [21] also presented that SMAs in braced frames, steel and concrete beam to column connections, as well as RC structure for reinforcing can be used successfully for energy dissipation, self-adapting, and healing of structures.

A Rocking wall system, which is one of the self-centering systems, has been studied for reducing overturning moment caused by seismic load. The post-tensioned rocking walls with viscous fluid and steel damper were tested on the shaking table test, and residual deformations were minimal due to the re-centering contribution from the rocking walls [22]. Additionally, for reliable performance-based seismic design, the rocking wall systems were modeled based on the plastic theory with bilinear plastic and linear elastic spring on joint region [23], and investigated to evaluate the dynamic response with sing degree of freedom oscillator [24,25]. Ferraioli et al. [26] suggested a continuous energy-dissipative steel column system which was a more promising strategy than the rocking wall system to retrofit existing building. A shear panel damper was considered as one of reliable energy dissipation device for earthquake energy. Especially, a low-yield strength steel or aluminum for the shear panel damper have been studied in terms of the hysteretic behavior according to the shear buckling of panel [27–29].

Marshall and Charney [30] investigated steel structures retrofitted with buckling-restrained braces in-series with viscoelastic dampers. Tsai et al. [31] introduced a combined damping system in which displacement- and velocity-dependent devices were used for cost-effective retrofitting. Lee and Kim [32], Lee et al. [33] and Eldin et al. [34] showed that hybrid dampers developed by combining friction and steel slit friction dampers were effective in reducing the residual deformation under medium-level earthquakes. Naeem et al. [35] developed and used a hybrid slit damper in which a conventional steel slit damper was combined with two diagonally arranged shape memory alloy bars. Eldin et al. [34] compared the life cycle cost of a hybrid damper with that of a viscous damper. Pekcan et al. [36] proposed a damped cable system in which a preloaded viscous damper was connected in series with a prestressed tendon, and found that the system was highly effective under pulse-type ground motions. Sorace and Terenzi [37,38] and Naeem and Kim [39,40] improved further the damped cable concept, conducted full-scale dynamic tests, and developed a preliminary sizing criterion and analytical model of this system.

The strengthening systems discussed above demonstrated high capabilities for minimizing residual displacement and inter-story drifts under an earthquake event. However, several of these systems are either expensive or require special technical skills for manufacturing and on-site installation. Steel bracing systems are considered a simple and economical retrofitting scheme; nevertheless, the system has its own limitations, such as local buckling if braces have thin cross-sections, or less economy when thick sections are used to avoid buckling. To avoid these limitations, an economical damped brace with a simple friction damper is proposed in this study. The steel brace splices were modified, converted into a friction damper, and tested under dynamic loading conditions. The proposed simplified damped braces were installed as diagonal or inverted-V (chevron) bracing in an RC frame, and the seismic



**Fig. 1.** Soft-first-story buildings in Korea (left), column shear failure in Pohang earthquake (right).

performance of the retrofitted systems was evaluated through shaking table tests. The effectiveness of the damping device was evaluated by comparing the test results of the retrofitted frames with those of the bare RC frame under identical loading conditions. The dynamic test results demonstrated that the proposed damper was effective not only in dissipating seismic energy, but also in reducing the potential local buckling failure in conventional braces. The friction-damped brace effectively reduced the displacement demands generated by the seismic input motions. This damping system may be an effective and economical retrofitting solution for low-to-medium-rise residential and public office buildings with soft first stories, such as the abovementioned buildings in Korea.

## 2. Details of proposed friction damper

### 2.1. Working mechanism

The friction damper proposed in this study was designed such that it fits as a conventional bolted-splice steel brace connection, requiring minimal on-site technical expertise. A typical splice of steel braces was converted into a friction damper, hereafter called “Bolted-Splice Friction Damper” abbreviated as “BSFD.” Fig. 2 shows the detailed schematic drawings of a BSFD. The main components of a BSFD are splice plates with designed long slot holes, steel bolts, washers, and steel nuts, along with conventional brace elements. Similar to steel splices, the BSFD connects the collinear brace elements with additional splice steel plates on top of both flanges with long slot holes, steel washers, steel bolts passing through them, and steel nuts at the bottom of the flanges. The splice plates were designed with long slot holes to provide slip friction between the plates and brace element. The connecting bracing components are provided with a gap by cutting them shorter in length in the connection region, which allows for collinear movement between the plate and brace. The gap between the brace elements, hereafter called, “stroke of BSFD” is determined in accordance with the maximum acceptable story drift ratio of 1%, recommended by the ASCE 41 guidelines [41] for life safety limit state of ordinary RC moment frames. The length of the long slot on the splice plates corresponded to a 1% story drift.

Fig. 3 presents the three-stage load-slip/displacement behavior of the proposed friction-damped brace system. Under lateral loads, the damped brace initially attracts a lateral load until it reaches the point where the relative slip between the splice plate and brace elements begins. The corresponding force and displacement are termed as  $f_i$  and  $\delta_i$  with stiffness  $k_i$ . Once the slip starts, the friction damper dissipates the seismic energy by converting it into heat and sound generated by the friction of the splice plates with brace elements. The base shear demand on the system does not increase further ( $f_{slip} = f_i$ ), until the slip displacement  $\delta_{slip}$  becomes equal to the designed stroke of BSFD. At this point, the gap between the brace elements becomes nearly zero, and the bearing mechanism starts. Afterward, the friction damper starts working as a conventional bearing connection of a conventional brace system and the damped brace starts resisting the lateral load until it reaches to its full force capacity  $f_u$  and corresponding displacement of  $\delta_u$ .

### 2.2. Cyclic tests of damper

The hysteresis behavior and energy-dissipation capacity of the proposed damper were evaluated using reversed cyclic loading tests. The coefficient of friction ( $\mu$ ) was determined and later used to estimate the friction force at which the damper starts to slip and dissipate energy. Three BSFD-based damped brace prototypes are tested using axial cyclic loading protocols. The tests were performed using a 3000 kN (675 kips) Universal Testing Machine (UTM). Fig. 4 shows the test setup and instrumentation used. The test specimens were designed with SM355 (A36) material and an H-shaped 200 × 200 × 8 × 12 steel section as the main brace elements. To allow inline movement without butting the brace elements, the stroke of the BSFD was designed to be 30 mm (1.18 in), which corresponds to a 1% drift ratio. The thickness of cover plate was 10 mm (0.4 in). The designed slot holes were 50 mm (1.97 in) long which could accept bolts (M20) with a diameter of 22 mm (0.86 in). Overall, the three test specimens were designed to have the same dimensions, except for the number of bolts and initial bolt force. Four load cells were installed between the bolt head and fender washer to measure the

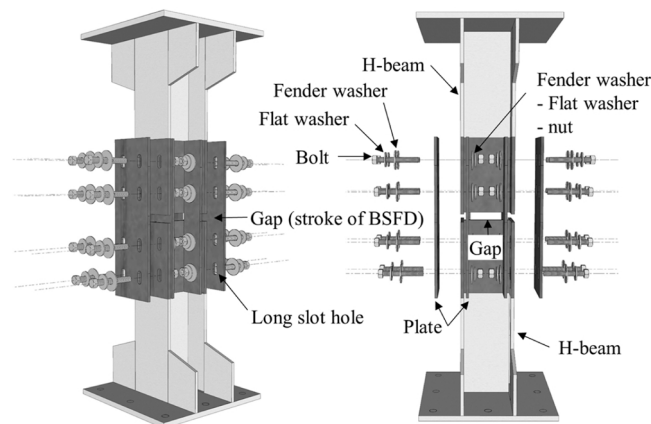


Fig. 2. Schematic of a damped brace with BSFD.

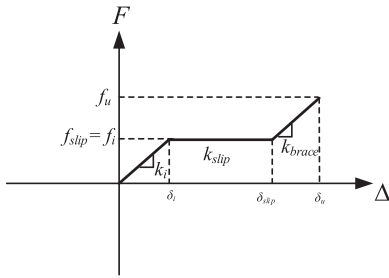


Fig. 3. Three-stage load-displacement behavior of proposed damped brace with BSFD.

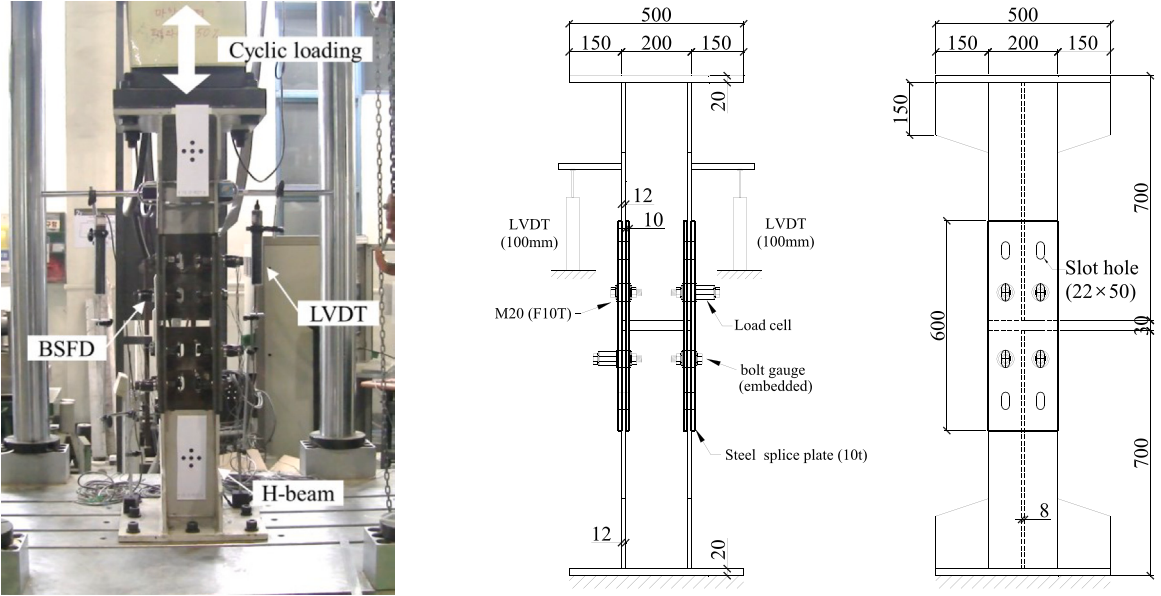


Fig. 4. Test setup and instrumentation of cyclic test specimen.

pre-tension force of the bolts during the tests. Table 1 lists the details of the specimens. In the specimen names, FD stands for friction damper; 4 and 8 are the number of bolts used; and 0.25 and 0.50 are the amount of initial tensile forces (in kN) applied to the connection bolts in terms of friction of the bolt tensile strength. To prevent potential buckling of the brace elements, the specimens were designed with slip loads approximately equal to 20% and 40% of the buckling capacity of the brace elements. The connection bolts were subjected to an equivalent initial tension force ( $T_i$ ), which was calculated using Eq. (1);

$$R_n = \mu T_0 N_s N_b \quad (1)$$

where  $R_n$  shows the friction force;  $\mu$  is the coefficient of friction which was initially assumed to be 0.4 for steel-to-steel surfaces;  $T_0$ ,  $N_s$ , and  $N_b$  show the minimum fastener tension force, the number of slip planes and the number of bolts, respectively.

The initial bolt force  $T_b$  was taken as  $0.25T_0$  and  $0.50T_0$  where  $T_0$  is the minimum fastener tension defined in KDS [42] and is similar to  $T_b$  of AISC [41] of M20 (A490M) bolts. Fig. 5 shows the loading protocol for the reversed cyclic loads in accordance with ASTM 310 [43]. The reversed cyclic loading protocol was specified to have four axial displacement amplitudes obtained from corresponding structural drifts of 0.25%, 0.5%, 0.7%, and 1%. The test specimens were subjected to six axial loading cycles at each displacement amplitude.

**Table 1**  
Details of specimens used in cyclic load tests.

No.	Specimens	Bolt size	$\mu$	$N_b$	$T_0$ (kN)	$T_i$ (kN)	$T_i/T_0$	$N_s$	$R_n^*$ (kN)
1	FD-4-0.25	M20(A490M)	0.4	4	179	40	0.22	2	128 *
2	FD-4-0.50		(assumed)	4		80	0.45		256
3	FD-8-0.50			8		80	0.45		512

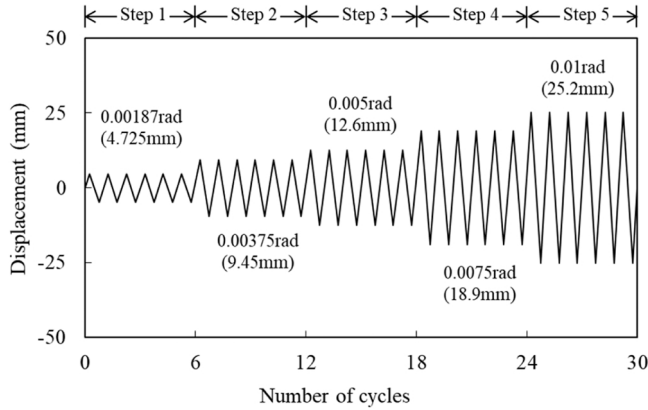


Fig. 5. Cyclic loading protocol used in prototype tests.

$R_i^*$  is based on Eq. (1) and  $\mu T_i N_s N_b = 0.4 \times 40 \times 2 \times 4 = 128$  kN.

### 2.3. Results of cyclic tests

Fig. 6 shows the cyclic test results. Overall, the hysteresis loops exhibited stable behavior under cyclic loads and dissipated seismic energy without pinching. In general, as the number and initial tension force of the bolts increased, the corresponding friction force or force required to initiate the slip increased. In specimen FD-4-0.25 with 4 bolts and  $0.25T_o$  initial tension force, the slip started at axial force of 96 kN (21.6 kips), whereas in FD-4-0.50 with 4 bolts and  $0.50T_o$ , the slip started at 179 kN (40.3 kips) of axial force which was 1.86 times higher than that of the specimens with  $0.25T_o$ . In specimen FD-8-0.50 with 8 bolts and  $0.50T_o$ , the load corresponding to the

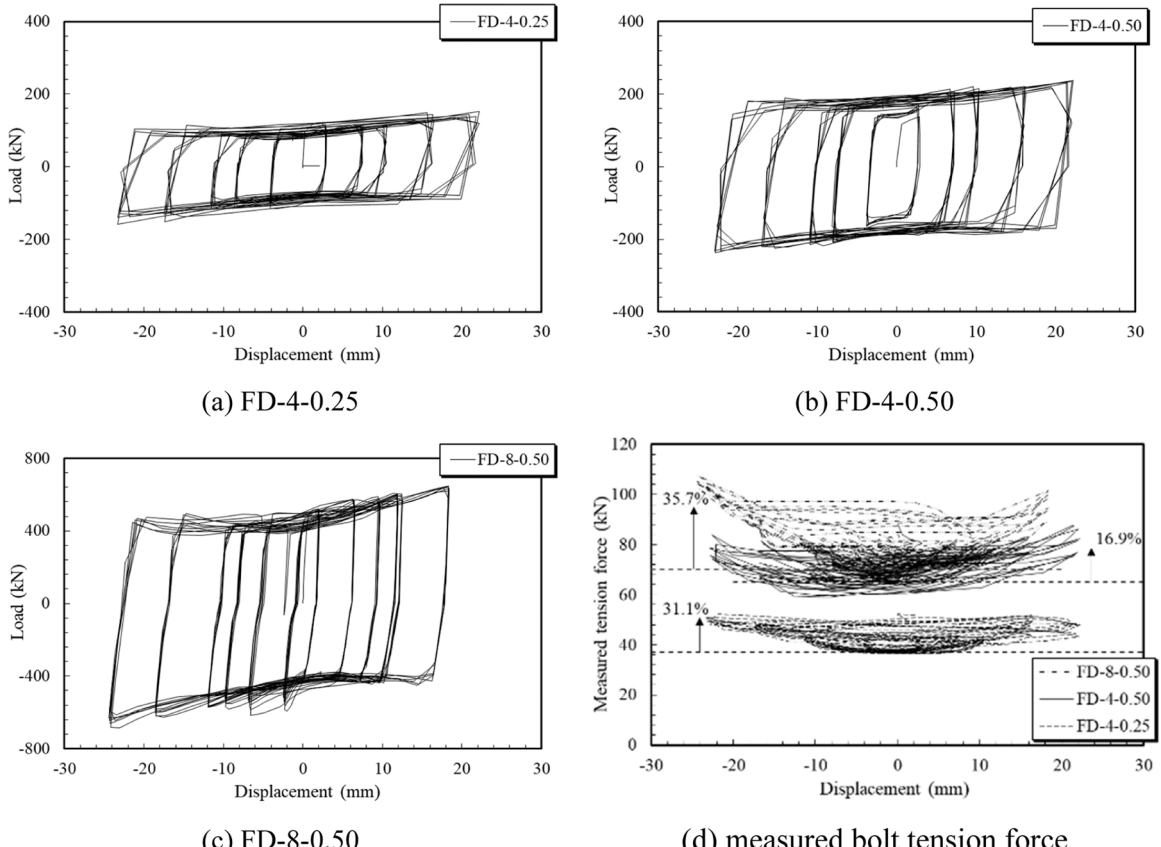


Fig. 6. Cyclic test results of damped brace with BSFD.

slip was 474 kN (106.6 kips). This indicates that if the number of bolts is doubled, the required friction force increases by more than 2.5 times.

As expected, after reaching the slip load, the dampers started dissipating seismic energy. For the maximum displacement amplitude of 25.2 mm (0.98 in) which was less than the designed stroke of 30 mm (1.18 in), the load-displacement relationship of the FD-4 specimen exhibited a nearly linear slip behavior with a negligible increase in force, as expected, and shown in Fig. 3. However, for drift ratios greater than 1% or an axial displacement of 30 mm (1.18 in), it is expected that the brace members will butt and carry an axial load, similar to a conventional steel brace. In the load-slip behavior of the FD-8–0.50 specimen, the stiffness increased slightly, as shown in Fig. 6(c). This may be associated with the increasing bolt force of FD-8–0.50, as shown in Fig. 6(d). More wear was also observed on the friction surfaces, as shown in Fig. 7. During the tests, the splice plate deflected out-of-plane owing to the vibration in the dampers with four bolts that impeded the slip. Therefore, it is recommended to use at least eight bolts on each flange and four on each side to avoid out-of-plane movement of the splice plates. Finally, the coefficient of friction was determined from the experimental results using Eq. (1) for each loading step. Table 2 shows the average friction coefficient values considering all the loading steps of the test specimens, which were calculated to be 0.384, 0.319, and 0.451 for specimens FD-4–0.25, FD-4–0.50, and FD-8–0.50, respectively.

### 3. Dynamic test of RC frames

#### 3.1. Test specimen details

Four one-bay single-story RC frames mimicking the non-seismic design of existing buildings were tested under dynamic loads. To ensure that the BSFD started to slip before the bare frames reached their capacity, friction dampers were designed with slip loads lower than the nominal capacity of the bare frames. As reported earlier [42], the friction coefficient for steel-steel surfaces varies over a wide range of 0.25–0.48; therefore, a large variation may be expected in the estimated slip load. For mill-scale conditions, AISC standards [41] recommend an average value of 0.30. A friction coefficient of 0.319 was chosen in tests which was the lowest value obtained in the cyclic tests but close to the mean value of 0.30 for class-A surfaces, (the unpainted clean mill scale steel surfaces) in AISC standards. The two main parameters of the shaking table tests were 1) the design slip load, which was taken as the ratio of the slip load to the bare frame strength, and 2) the brace type. The tests were intended to evaluate the effect of three levels of design slip load: 50%, 80%, and 90% of the flexural capacity of the RC frame, and the effectiveness of the BSFD with two brace types: diagonal and chevron braces, as shown in Fig. 8. All BSFDs used in this study were designed with eight bolts, as shown in Fig. 4.

The test specimens are presented in Table 3. The tested frames were named according to their designs and retrofitting schemes. In the specimen names, NS represents the non-seismic design of RC frames; the two letters after it show the arrangement of damped braces: DF represents a diagonal brace with BSFD, and AF represents an inverted-V (chevron) brace with BSFD; The numbers 0.50, 0.80, and 0.90 are the ratio of the slip load to the flexural capacity of the bare frame. The slip load of BSFD was calculated using Eq. (1), assuming  $\mu = 0.319$ ,  $N_s = 2$  and  $N_b = 8$ . The minimum fastener tension force  $T_o$  was adjusted to achieve the target slip load corresponding to 50%, 80%, and 90% of the nominal flexural capacities of the bare frames in specimens NS-DF-0.50, NS-DF-0.80 and NS-AF-0.90, respectively.

The test specimens were designed using a column-yielding philosophy, which was a non-seismic approach for seismic retrofitting by BSFD. As shown in Fig. 9, the NS specimen (bare frame) was a one-bay single-story RC frame consisting of two columns (left and right), a top (roof) beam, and a strong bottom (footing) beam. The cross-sectional dimensions of the columns were 400 mm × 400 mm (15.75 in × 15.75 in), whereas the top and footing beams had a cross-section of 350 mm × 550 mm (13.8 in × 22.6 in) and 500 mm × 500 mm (19.7 in × 19.7 in), respectively.

The total frame height was 3.85 m (12.63 ft) and the clear height of the columns was 2.75 m (9 ft). The total width of the frame was 4.5 m (14.76 ft), with a clear beam span length of 2.9 m (9.51 ft). The columns were designed with D16 (#5) rebars having a sectional area of 201.1 mm<sup>2</sup> (0.31 in<sup>2</sup>), with three on each side as the flexural tension and compression reinforcements. The top beam was designed with 4-D22 (4#7) rebars, and the bottom beam had 6-D22 (4#7) rebars for flexural tension and compression reinforcement. The columns were designed with a D10 (#3) bar as shear stirrups at a center-to-center spacing of 300 mm (11.8 in). The top and bottom

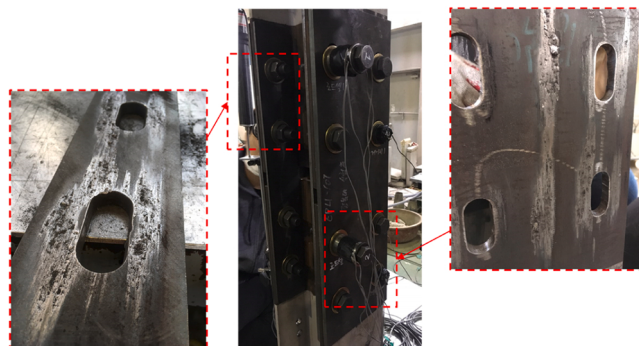
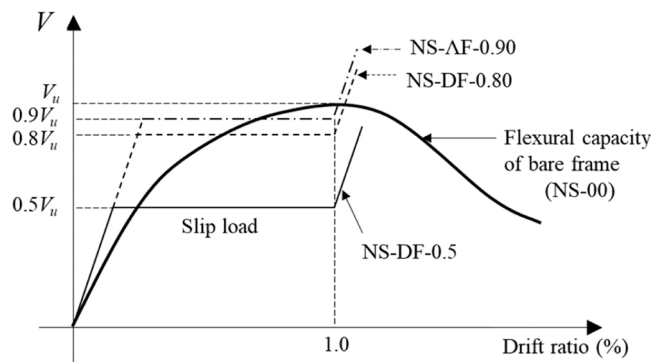


Fig. 7. Damage to the surface of splice and H-beam of BSFD.

**Table 2**

Estimated friction coefficient at each displacement step during cyclic tests.

Specimen	Friction Coefficient ( $\mu$ )					Average
	Step 1	Step 2	Step 3	Step 4	Step 5	
FD-4-0.25	0.348	0.344	0.345	0.436	0.449	0.384
FD-4-0.50	0.252	0.321	0.327	0.338	0.354	0.319
FD-8-0.50	0.423	0.454	0.446	0.450	0.482	0.451

**Fig. 8.** Design slip load of BSFD taken as percentage of bare frame strength.**Table 3**

Test specimens.

Specimen	Brace Type	Number of BSFD	Bolt ( $T_o$ )	Friction coefficient ( $\mu$ )	$N_s$	Initial bolt tension force ( $T_i$ )	$T_i/T_o$	Estimated slip force, $R_n$ (kN)
NS-00	-	-	-	-	-	-	-	-
NS-DF-0.50	Diagonal	1	8-M20 (179 kN)	0.319	2	40	0.22	204.2
NS-DF-0.80	Diagonal					65	0.36	331.8
NS-AF-0.90	Chevron	2				30	0.17	306.2

beams had stirrups with D10 (#3) rebars spaced at 300 mm (11.8 in) and 200 mm (7.87 in), respectively. The box-type connection zone component for the NS-DF test specimen (Fig. 9(b)) was fabricated using SS400 steel. It is connected to the bottom (footing) beam with 9-M16 anchor bolts and also connected to the column with 9-anchor bolts, resulting in a total of 18 anchor bolts used per corner component.

Material coupon tests were conducted before shaking table tests were conducted on the RC frames. Table 4 presents the designed sections and material properties of the tested RC frames. In accordance with ASTM guidelines [43], dog-bone-shaped coupon test specimens were prepared for damper materials, direct tension test specimens for rebars were prepared and tested, and compression tests on concrete cylinders were conducted to measure their strengths. The measured yield strength of flexural reinforcement of columns and beams were 521.2 MPa (75.6 ksi), and 503.3 MPa (73.0 ksi), respectively. The shear stirrup reinforcements exhibited a measured yield strength of 403.4 MPa (58.51 ksi). The H-steel brace and steel plate used in the damper had a measured yield strength of 282.3 MPa (40.95 ksi) and 274.6 MPa (39.82 ksi), respectively. The average compressive strength of concrete  $f'_c$  after 28 days of testing through cylinders was 16.9 MPa (2.45 ksi).

The basic RC frames of NS-DF-0.50 and NS-DF-0.80 had the same material and sectional properties but were retrofitted with a diagonal damped brace with a BSFD. The connection zones of the diagonal braces with the concrete were prepared by welding the steel plates in a box shape, as shown in Fig. 9(b). The box-shaped connection zone was anchored at the lower-left and upper-right corners of the frame by drilling and inserting anchor bolts. The brace elements were connected through a splice at the top-right end. At the lower-left end, the splice was converted to a BSFD. The high-tensile (A490M) bolts were provided with an initial fastener tensile force of either 40 kN (9.0 kips) or 65 kN (14.6 kips), which was nearly  $0.22T_o$  or  $0.36T_o$  to achieve target slip loads corresponding to 50% and 80% of strength of bare frames. Fig. 10 presents the details of the NS-AF-0.90 specimen that was retrofitted with two BSFDs arranged at the lower ends of chevron braces. The brace elements composed of H-shaped ( $200 \times 200 \times 8 \times 12$ ) steel sections were welded in an inverted V shape (with a C-shape  $200 \times 90 \times 8 \times 13.5$ ) steel section having.

length equal to the length of top beam of the frame. Another C-shaped section was welded with H-shaped short-brace elements at both ends, with an inclination equal to the angle of the braces. Subsequently, the two C-shaped steel sections were fixed with top and bottom beams of the RC frames by using M16 anchors. Finally, the upper long and lower short inverted-V brace elements were connected using two BSFDs. The bolts of the BSFD were provided with an initial tensile force of  $0.17T_o$ , designed for a slip load equal to

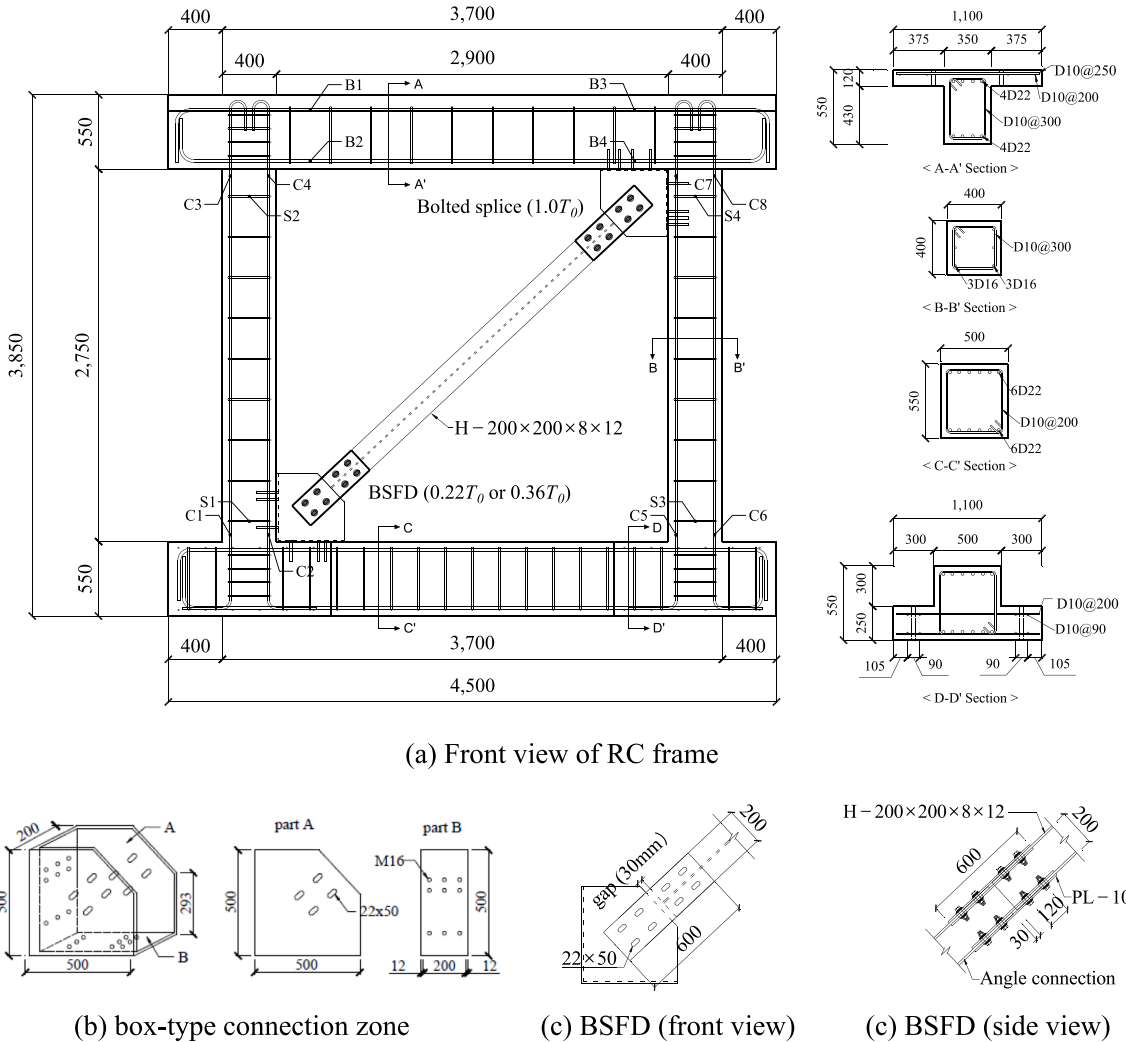


Fig. 9. Details of a retrofitted frame by diagonal brace-type BSFD (NS-DF specimen).

Table 4

Material and sectional details of non-seismically designed compliant RC frame.

Components	Beam	Column	Footing Beam
Cross-section (mm)	350 × 550	400 × 400	500 × 500
Flexural reinforcement	Top: 4-D22 Bottom: 4-D22	3-D16 3-D16	6-D22 6-D22
Shear Stirrups	D10 @ 300	D10 @ 300	D10 @ 200
Aver. measured $f_y$ (MPa) of D10 rebar	403.4	403.4	403.4
Aver. measured $f_y$ (MPa) of D16 rebar	-	521.2	-
Aver. measured $f_y$ (MPa) of D22 rebar	503.3	-	503.3
Aver. measured $f_c$ (MPa)	16.9	16.9	16.9

90% of nominal flexural capacity of bare frame.

### 3.2. Test setup and instrumentation

Fig. 11 shows a photograph of the test setup and instrumentation used in this study. First, the tested frame specimens were fixed on a shaking table using hydraulic nuts, and then bracing systems were installed. To simulate the effect of the top-floor weight, a mass of 22 t was fixed on top of the upper beams using anchors. The lateral load was measured by installing four load cells on the lower floor.

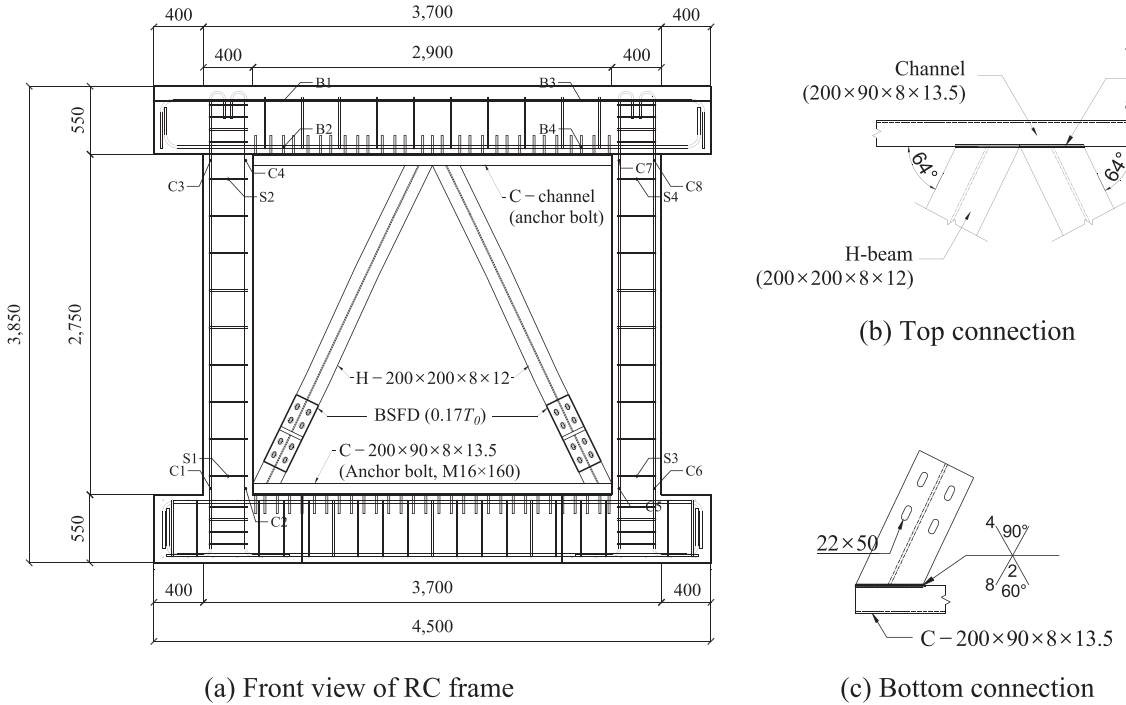


**Fig. 10.** Details of a retrofitted frame by chevron brace type BSFD (NS-AF specimen).

Linear variable differential transducers (LVDT) were installed at the upper- and lower-right ends of the specimen to measure the frame displacement. In addition, four accelerometers were installed to measure the acceleration at the bottom of the shaking table and at the top, middle, and bottom of the right column. To measure the strain in the flexural and shear reinforcements of the column and beams, the strain gauges C1~C8, B1~B4 and S1~S4 were attached as shown in Figs. 9 and 10.

### 3.3. Input ground motion

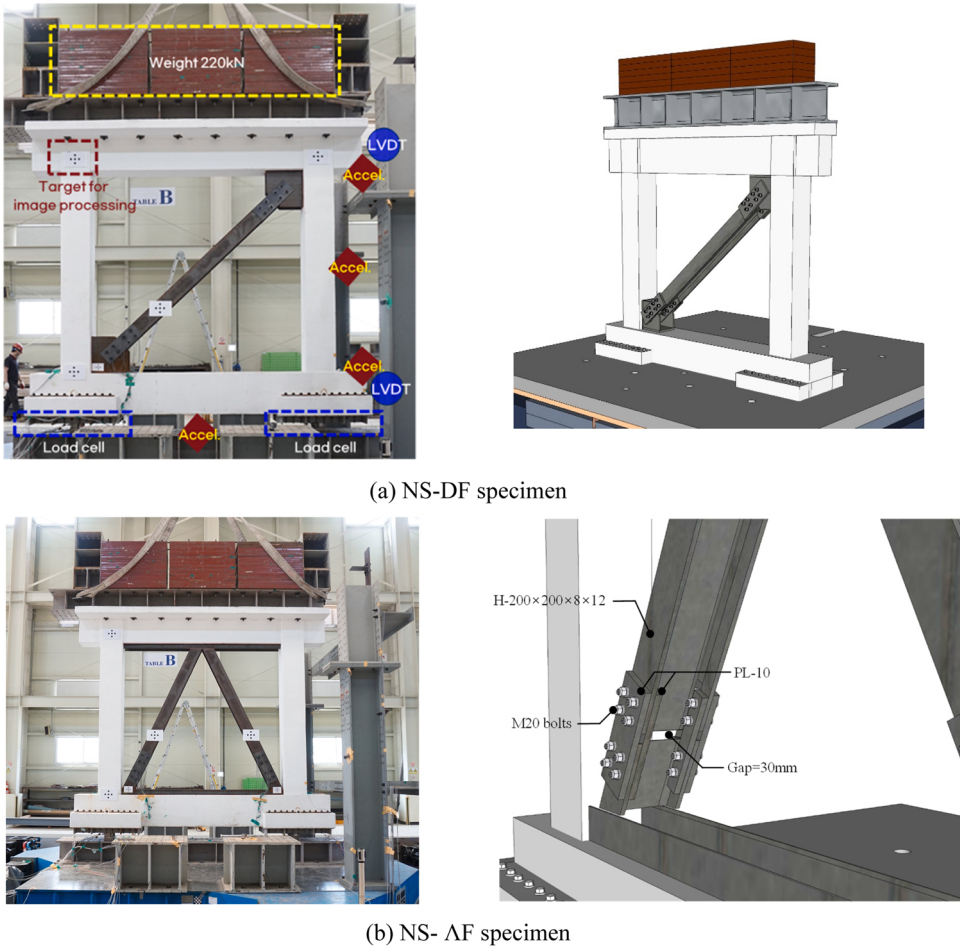
The Gyeongju and Pohang earthquakes in 2016 and 2017 with respective magnitudes of 5.8 and 5.4, occurred for a very short duration of high intensity (2 s only) with a total period of 20 s. To understand the dynamic behavior of the structures subjected to Korean earthquake characteristics, artificial seismic waves with dynamic traits similar to the response spectrum by the KDS41-17 Seismic Design Standard [44] for the S4 soil type, seismic grade-1, and a damping ratio of 5% were created. Fig. 12 presents a time-acceleration graph of the artificial seismic wave used in this study. The peak ground acceleration (PGA) was 0.236 g, and the intense earthquake duration was approximately 20 s. Fig. 13 shows the response spectrum of the artificial seismic wave compared to the response acceleration spectrum (damping ratio,  $\xi = 0.05$ ) of the S4 soil type. Shaking table tests were performed using eight earthquake levels (EQ-levels in percentage of PGA) with corresponding ranges of PGA, as shown in Table 5.

## 4. Dynamic test results

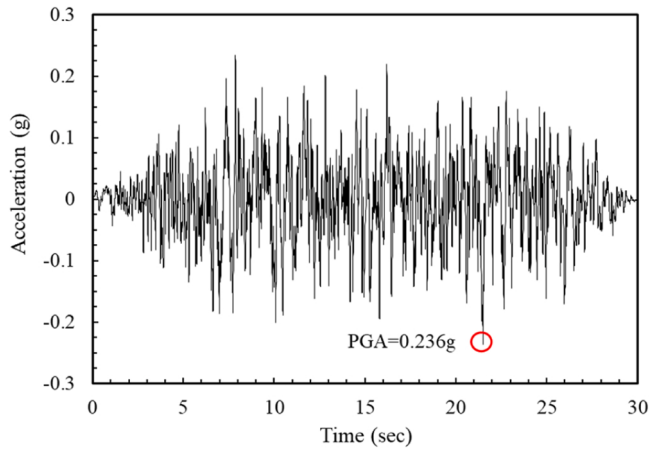
### 4.1. Cracking pattern and failure modes

Fig. 14 shows the cracking patterns of the test specimens at the end of the final excitation. In specimen NS-00 at EQ-50%, the flexural cracks started developing at both ends of left column, and at top end of right column. With increasing EQ levels, the width of the column flexural cracks increased, and new cracks developed. When the specimen was subjected to EQ-150%, an inclined shear crack appeared in the left upper beam-column joint region, the width of which further increased until the test was terminated at EQ-190%. Flexural bar slip was also observed at the lower-right end of the column at the ultimate load. Overall, the cracks were primarily concentrated within the plastic hinge regions of the columns, except for a major joint shear crack under higher levels of input motion that propagated toward the top beam. This cracking pattern indicates that the NS-00 specimen failed due to column flexural tension failure, which was confirmed from the measured strain of the flexural rebar, as shown in Fig. 15.

In retrofitted specimens NS-DF-0.50 and NS-DF-0.80, flexural cracks started to develop first at the midspan regions of the top beam for lower levels of EQ. As the EQ level increased, the beam flexural crack width increased, became slightly inclined, and propagated upward to the flexural compression zone. Near EQ-250%, flexural cracks appeared at the upper end of the left column, and bond cracks near the connection zone of the brace developed at EQ-300%. For specimen NS-AF-0.90, flexural cracks mainly appeared in region



**Fig. 11.** Test setup of NS-DF and NS-AF specimens.



**Fig. 12.** Acceleration of artificial wave.

right from the mid-span point of top beam where brace was connected. A smaller number of cracks appeared under higher levels of input ground motion compared with the diagonally braced frames. The beam cracks propagated slightly upward with increasing EQ levels, and flexural cracks developed at the top end of the right column. Finally, at EQ-250%, a major bond crack developed at the right end of the lower beam near the brace connection, as shown in Fig. 14(d). The column flexural strain data in Fig. 15 show that the

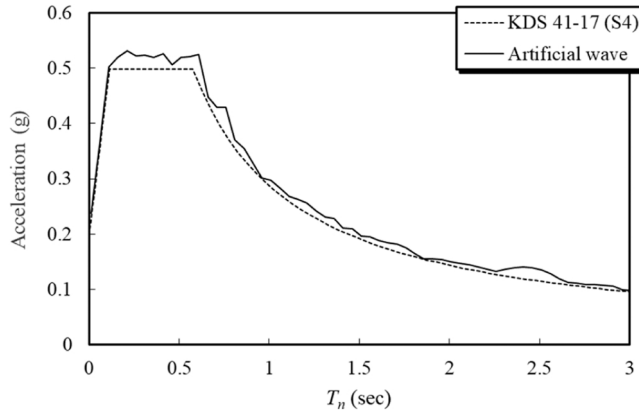


**Fig. 13.** Response spectrum of artificial wave.

**Table 5**  
Loading steps for dynamic test as percentage of PGA.

Step	EQ level	PGA (g)
1	50%	0.118
2	80%	0.189
3	100%	0.236
4	150%	0.354
5	200%	0.472
6	250%	0.590
7	300%	0.708
8	350%	0.826

column flexural reinforcement remained elastic for all retrofitted structures, even under higher EQ demands, except for specimen NS-DF-0.90, in which the flexural rebar yielded at EQ-350%. Although the beams did not reach their yielding strain, the cracking pattern and measured strains in the flexural reinforcement indicated that the damped brace system successfully shifted the cracking and damage concentration from the columns to the beams.

#### 4.2. Base shear vs. story drift

In general, the base-shear vs. story drift behavior of the test specimens showed that the retrofitting schemes effectively reduced the story drift demand even for higher levels of EQ compared to the bare frame. Fig. 16 compares the base shear vs. drift ratios of the three retrofitted test specimens with behavior NS-00 at EQ-200%. In the case of NS-00, the test was terminated when the input ground motion reached EQ-190% because the drift ratio was nearly 2.5%, and a total collapse of the frame was expected, which could damage the test facility. For the selected EQ-200%, the retrofitted structures showed high initial stiffness and reduced lateral drift compared with the bare frame. The retrofitted structures showed no sign of stiffness change for the selected EQ level, which indicated that the brace absorbed seismic energy, and the system showed a very low drift ratio of less than 0.5%. The braces increased the initial stiffness up to 3.79 times higher than that of NS-00. The maximum base shear at EQ-200% was 181.6 kN (40.8 kips) for NS-00, 233 kN (52.4 kips) for NS-DF-0.50, 373.6 kN (84.0 kips) for NS-DF-0.80 and 397.2 kN (89.3 kips) for NS-ΔF-0.90 specimen, respectively. To better understand this behavior, the base shear vs. drift ratio curves of the maximum values corresponding to each EQ level were obtained and are presented in Fig. 17.

The maximum base shear and drift ratios were determined by plotting the corresponding values against the time history of each EQ level. The markers in the graphs correspond to the EQ levels. In general, the NS-00 specimen exhibited typical ductile RC frame behavior. The weak column members yielded first at EQ-100% (approximately 0.8% drift ratio) and formed plastic hinges that continued to sustain the maximum load in the post-peak loading range with a slight degradation up to a drift ratio of nearly 2.5%. Such behavior is generally expected when plastic hinges are formed in the beams. However, it was not unexpected because as reported earlier [45–47], under low axial force ratios ( $n$ ), the columns show higher ductility without pinching ( $n = P/A_g f_c$ , where  $P$  is the axial compressive force,  $A_g$  is the gross area of cross-section, and  $f_c$  is the concrete compressive strength). Although a mass of 22 t was attached to the top beams, the  $n$  remained less than 5%. All the retrofitted structures exhibited similar stiffness until an EQ of 100%. However, specimen NS-DF-0.50, started to show some stiffness reduction and nonlinear behavior because cracks developed at the mid-span of the top beam. At EQ-250% (drift ratio of approximately 0.5%), the specimen exhibited a plateau in the base shear-drift behavior until the drift reached 1%. This plateau corresponds to the point at which the BSFD started to slip and dissipate seismic energy. After a 1% drift ratio, buckling of the braces occurred as expected in the design, and the braces started to carry further load, as shown by the solid line. Before the BSFD started to operate, the stiffness remained almost the same with the brace system, and a

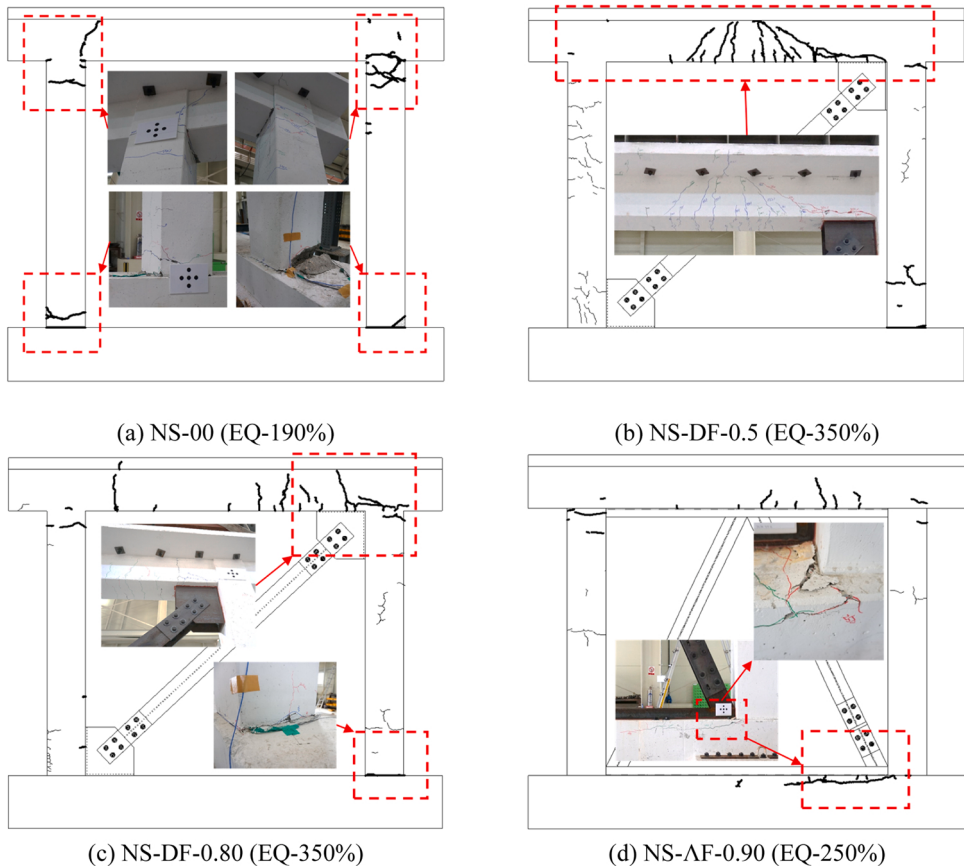


**Fig. 14.** Crack patterns at the end of the final excitation.

decrease in stiffness and an increase in deformation occurred clearly at the EQ level at which the BSFD operated. In specimens NS-DF-0.80 and NS-AF-0.90, the braces absorbed seismic energy for large EQ levels and attracted higher base shear with low drift ratio of nearly 0.5%. This was expected, because the BSFDs of these specimens were designed with higher slip loads than those of NS-DF-0.50. In the case of NS-DF-0.80, the nonlinear behavior started at EQ-200% due to cracking in the top beam, the BSFD started to slip when it reached EQ-300%, and a plateau appeared in the shear-drift behavior until the final input value (EQ-350%) corresponding to a 0.6% drift ratio. Although the test was stopped here, it was expected that a clear plateau would continue until the drift reached 1% if the structures were subjected to higher levels of input ground motion. Specimen NS-AF-0.90 showed a slightly low stiffness after EQ-150% than NS-DF-0.80 and showed a sharp reduction in base shear after reaching EQ-250%, contrary to the expectation that the BSFD would start to slip and dissipate energy. This may be associated with the large cracks appearing at the lower-end connection zones of the damped braces, and the test was terminated at EQ-300% to avoid sudden collapse.

Fig. 18 shows the base shear and drift ratio responses according to the time history of the final input excitation for each specimen. As shown, the ultimate drift ratios of the retrofitted structures were significantly reduced, even for higher earthquake demands (EQ-300% or -350%). However, the base shear increased in the retrofitted frames and absorbed seismic energy. In particular, in specimen NS-DF-0.80 with a high initial bolt force ( $0.36T_o$ ), the damper started to slip and dissipate energy at higher ground motion level (EQ-300%), and in specimen NS-AF-0.90 with chevron braces, the attached friction dampers couldn't reach the slip load but test was stopped due to brace connection damage. Nevertheless, as shown in Fig. 18 (b), for specimen NS-DF-0.50 with  $0.22T_o$ , the BSFD reached the slip load and dissipated a significant amount of seismic energy, which helped to reduce the base shear demand. The damper continued to dissipate seismic energy without increasing the base shear until the test structure reached a drift ratio of 1%, based on which the BSFD stroke was designed.

#### 4.3. Variation in natural frequency

Fast Fourier Transform (FFT) was performed with white noise before all steps of seismic excitation to analyze the natural frequency and periods of the test specimens. Fig. 19 shows the frequency spectra of all the tested frames. The initial natural frequency of the NS-00 specimen corresponding to EQ-50%, was approximately 4.23 Hz. The natural frequency was slightly reduced after the initial cracking. With an increase in the input ground motion level, the natural frequency of the bare frame decreased dramatically due to cracking. At EQ-150%, shear cracks developed in the beam-column joint, and the natural frequency of NS-00 decreased sharply to

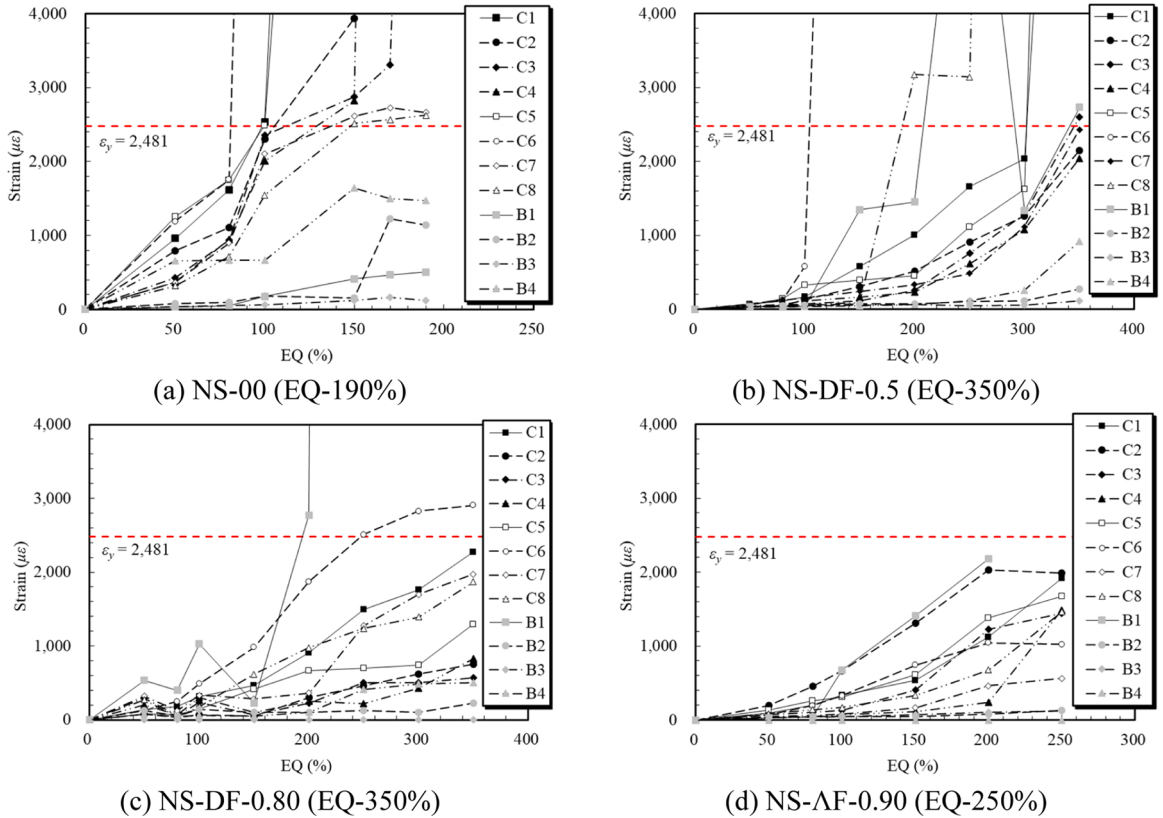


Fig. 15. Maximum strain values at each excitation.

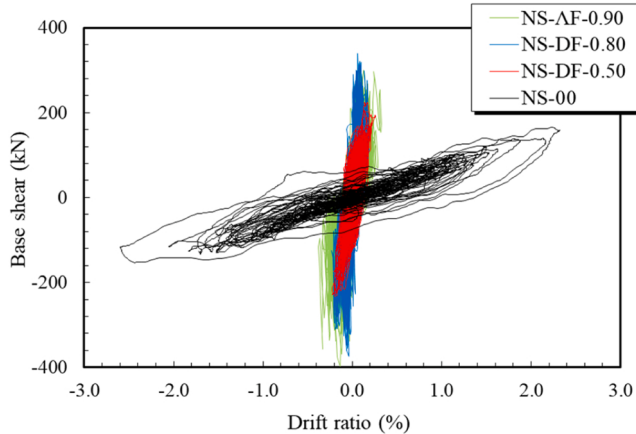


Fig. 16. Base shear vs. drift ratio at EQ 200% (EQ 190% for NS-00).

1.81 Hz. In contrast, the retrofitted structures exhibited a stable natural frequency, indicating that the systems incurred less cracking and damage. Initially both NS-DF specimens had a natural frequency of about 7.59 Hz, approximately 1.79 times higher than that of NS-00. Even after EQ-200%, there was no significant change in the natural frequencies of the two specimens. After EQ-250% and 300%, the natural frequency of NS-DF-0.80 and NS-DF-0.50 decreased to 4.86 Hz, which corresponds to cracking in top beams. The NS-AF-0.90 specimen had an initial natural frequency of about 7.14 Hz, which was approximately 1.68 times higher than that of NS-00. After EQ-200%, due to the large cracks in the bottom right brace connection zone, the natural frequency decreased to approximately 4.23 Hz.

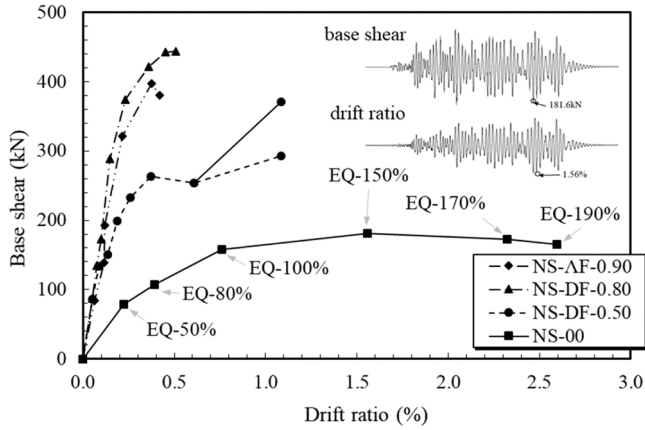


Fig. 17. Maximum base shear and drift ratio curves.

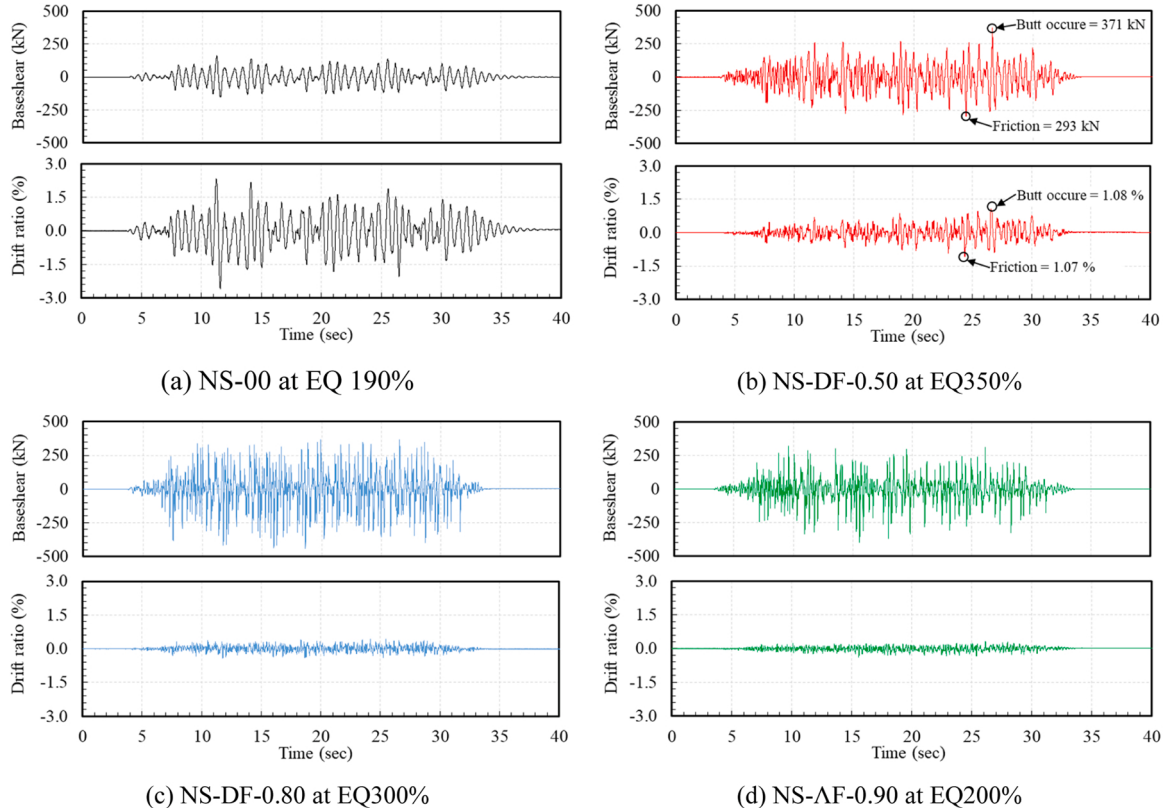


Fig. 18. Time history responses of base shear and drift ratio.

#### 4.4. Evaluation of energy dissipation capacity

Fig. 20 shows the energy dissipation capacities of the test specimens at a selected drift ratio of 0.4%. A 0.4% drift was chosen for a fair comparison, being the largest drift ratio of the specimens with higher slip loads. The energy dissipation capacity was calculated as the area under the hysteresis curve of the base shear force-drift ratio. In general, the retrofitted structures dissipated more energy than the non-retrofitted structures at the selected drift level. In the case of NS-00 specimen, the energy dissipation capacity was measured to be 2.4 kN·m (1.8 kip·ft) at 0.4% drift ratio. Specimens NS-DF-0.50 and NS-DF-0.80 had an energy dissipation capacity of 74.8 kN·m (55.2 kip·ft) and 54.4 kN·m (40.1 kip·ft), respectively. Specimens NS-DF-0.50, and NS-DF-0.80 dissipated more seismic energy than the other specimens because the BSFD started to slip and dissipate sufficient energy. NS-DF-0.80 exhibited sufficient energy dissipation capacity at the stage where the BSFD started to operate, but it was slightly lower than that of NS-DF-0.50. NS-AF-0.90 showed an

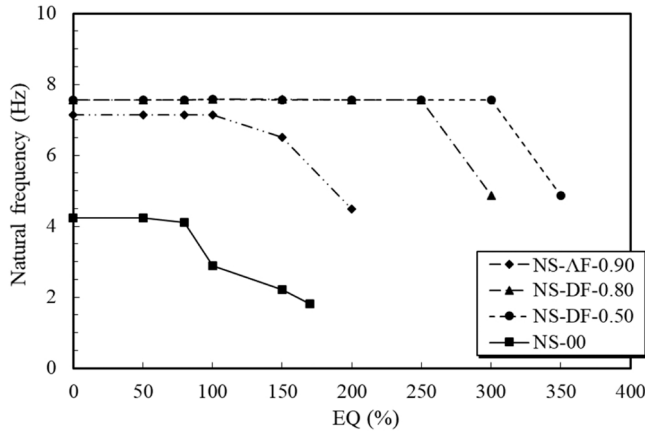


Fig. 19. Response frequency of specimens.

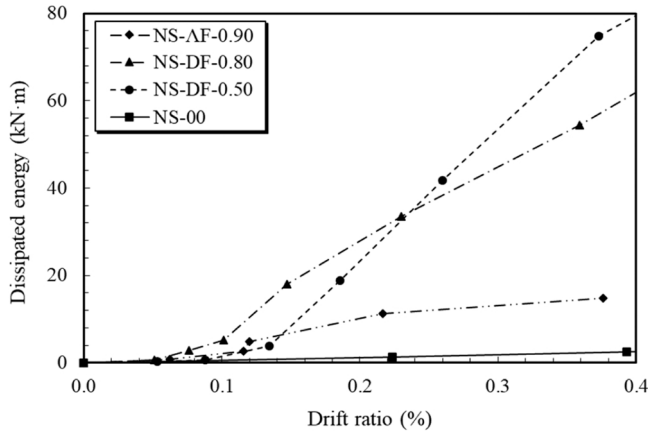


Fig. 20. Absorbed energy of specimens at drift ratio of 0.4%.

energy dissipation capacity of 14.7 kN·m (10.8 kip·ft) at the selected drift level. Its energy dissipation capacity was the lowest among all the retrofitted structures because the connection failure occurred before the start of the slip.

#### 4.5. Discussion

The design slip load of the friction damper was an important factor in the proposed retrofitting scheme. Although the proposed

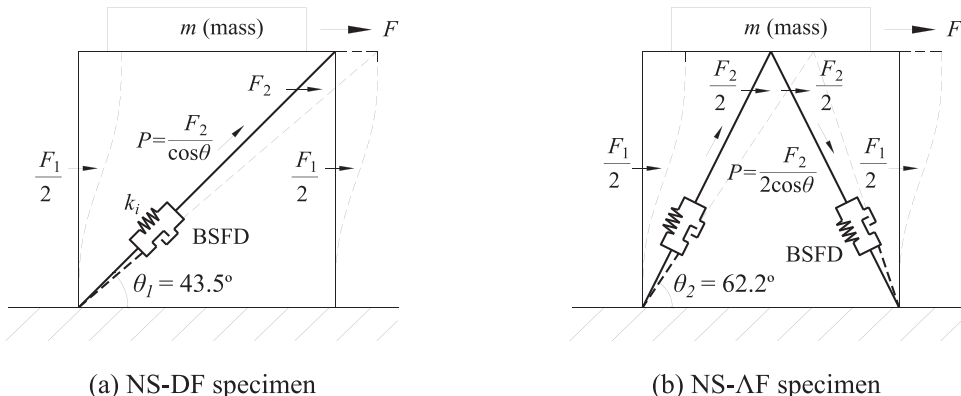


Fig. 21. Lateral force ( $F$ ) distribution mechanism.

system was effective in reducing the lateral drift demands, the base shear demand increased in the specimens with a higher designed slip load. A higher design slip load decreased the energy dissipation capacity because the full potential of the BSFD couldn't be utilized. Similar trends were observed when the BSFD was aligned with chevron brace.

For the retrofitted structures, it was assumed that the BSFD would start to dissipate seismic energy when the axial forces acting on the brace were equal to or greater than the design slip load. However, the results showed that the actual slip load was higher than the theoretically estimated load depending on the design slip load level. Fig. 21 shows the concept of force transfer in the damped brace system, where the lateral force ( $F$ ) generated in the frame acts as a shear force ( $F_1$ ) on the RC frame and transfers an axial force ( $P$ ) on the brace. Table 6 lists the measured axial force components of the base shear generated in the damped brace elements for each EQ level during the experiment. The axial force values with asterisks correspond to the estimated slip loads. The slip-force demands were calculated by transforming the flexural capacity of the bare frames. The slip load of specimen NS-DF-0.50 was estimated to be 204.2 kN (45.9 kips), whereas in specimens NS-DF-0.80 and NS-AF-0.90 the loads were estimated to be 331.8 kN (74.6 kips), and 306.2 kN (68.8 kips), respectively.

As shown in Fig. 22, in specimen NS-DF-0.50 with  $0.22T_0$ , as expected, the damper started to slip and dissipate seismic energy when the axial force reached 204.0 kN (45.8 kips), which corresponded to the estimated value. In specimen NS-DF-0.80 with  $0.36T_0$ , the damper started slipping at an axial force of 452.0 kN (101.6 kips), which was 1.36 times higher than the theoretically estimated value. In NS-AF-0.90 with  $0.17T_0$  and a chevron brace, the BSFD was expected start slipping at an axial force of 306.2 kN (68.8 kips), but the actual slip started at an axial load of 628.7 kN (141.3 kips) which coincided a sudden reduction in base shear due to a major crack at the bottom end of brace connection as discussed above. The shaded area under the curve represents the gap between the observed and expected slip loads calculated based on the average value of the friction coefficient. This indicates that a higher level of slip load should be expected than the theoretically estimated value, particularly for dampers with higher design slip loads, because the friction coefficient varies significantly. Grondin et al. [48] summarized test results of bolted joints and recommended an average slip coefficient of 0.31 for steel-steel surface with clean mill-scale condition. However, the largest slip coefficients and coefficients of variance (COV) in their reported experimental data were 0.483 and 0.255, respectively. Considering the variability of the friction coefficient for the proposed damped brace system with BSFD, it is recommended that the designed slip load not exceed 50% of the lateral load capacity of the bare RC frame.

## 5. Summary and conclusions

This study presents shaking table tests on RC frames retrofitted with a friction-damped brace. A three-stage load-displacement behavior of damped brace structures was introduced, in which retrofitted structures initially absorbed seismic energy until the load reached the designed slip load of the friction damper, at which point it started to slip and dissipate seismic energy without further increasing the base-shear demand. The observed crack patterns and measured strain values of the retrofitted specimens indicated that the damped brace system successfully shifted the damage concentration from the columns to the beams. More cracks developed, and flexural rebar strains increased in the top beams of the retrofitted structures than in the bare frame, in which flexural cracks developed in the columns. The lateral drift ratios of the retrofitted structures are significantly lower than those of the bare frames. The results indicate that the friction damper in specimen NS-DF-0.50 dissipated seismic energy without increasing the base shear until the slip displacement reached the design stroke. However, in NS-DF-0.80 with a design slip load of 80%, the damper began to slip at higher EQ levels, which increased the base shear demand. Similar, behavior was observed in specimen NS-AF-0.90 with chevron braces. The natural frequency of the retrofitted structures exhibited a more stable behavior than that of the bare frame because the systems incurred less structural damage. At a selected drift level, the retrofitted structures dissipated more seismic energy than the bare frame. At a drift ratio of 0.4%, specimen NS-DF-0.50 showed a higher energy dissipation capacity of 74.8 kN·m (55.2 kip·ft) than the bare frame with a capacity of 2.4 kN·m (1.8 kip·ft). The energy-dissipation capacity appeared to decrease with an increase in the design slip load. For example, NS-DF-0.80 showed a lower energy dissipation of 54.4 kN·m (40.1 kip·ft) for the same drift level than specimen NS-DF-0.50.

Before the BSFD operated, the RC frame behaved as strengthened by the brace system. After operating the BSFD, it dissipated the seismic energy and reduced the drift and the damage of the RC frame. Based on these observations, it can be concluded that structures retrofitted with the proposed damped-brace systems may show stable behavior with higher load redistribution and reduced seismic

**Table 6**  
Measured axial force acting on damped brace.

EQ scale (%)	Axial force, $P$ (kN)		
	NS-DF-0.50	NS-DF-0.80	NS-AF-0.90
50	92.3	94.8	132.6
80	140.8	148.3	209.1
100	142.2	188.4	322.3*
150	183.0	325.5	523.8*
200	204.0*	404.4*	628.7*
250	220.8*	441.3*	578.2*
300	161.6*	452.0*	
350	173.5*	441.6*	

\* axial load corresponding to start of damper slip.

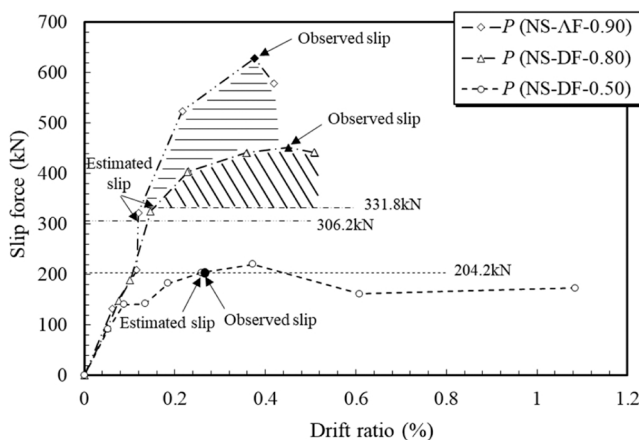


**Fig. 22.** Measured and estimated slip force ( $P$ ) of BSFD.

demands. The experimental and theoretical approaches were conducted on a one-bay single-story RC frame, which has limitations in applying continuous RC columns and beams. Therefore, the application and analytical study of the BSFD on multi-story structures remains in the future works.

#### Declaration of Competing Interest

The authors declare that they have no known competing financial interests or personal relationships that could have appeared to influence the work reported in this paper.

#### Data availability

Data will be made available on request.

#### Acknowledgments

This work was supported by the National Research Foundation of Korea (NRF) grant funded by the Korean Government (MSIT). (No. 2020R1A2C2102552).

#### References

- [1] M.A. Rahman, S. Sritharan, Performance-based seismic evaluation of two five-story precast concrete hybrid frame buildings, *J. Struct. Eng.* 133 (2007) 1489–1500.
- [2] D. Bedoya-Ruiz, C.A. Bermúdez, D.A. Álvarez, G.A. Ortiz, J.V. Escobar, Cyclic behavior of prestressed precast concrete walls, *Proc. 15th World Congr. Earthq. Eng., Lisbon, Port.* (2012) 19578–19585.
- [3] H.-S. Hu, J. Nie, M.R. Eatherton, Internal force and deformation of concrete-filled steel plate composite coupling beams, *J. Constr. Steel Res.* 92 (2014) 150–163.
- [4] M.R. Maher, A. Hadjipour, Experimental investigation and design of steel brace connection to RC frame, *Eng. Struct.* 25 (2003) 1707–1714, [https://doi.org/10.1016/S0141-0296\(03\)00162-7](https://doi.org/10.1016/S0141-0296(03)00162-7).
- [5] M.R. Maher, S. Yazdani, Design of steel brace connection to an RC frame using Uniform Force Method, *J. Constr. Steel Res.* 116 (2016) 131–140, <https://doi.org/10.1016/j.jcsr.2015.09.010>.
- [6] M.R. Maher, S. Yazdani, Seismic performance of different types of connections between steel bracing and RC frames, *Iran. J. Sci. Technol. - Trans. Civ. Eng.* 40 (2016) 287–296, <https://doi.org/10.1007/s40996-016-0034-z>.
- [7] H. Ghaffarzadeh, M. Maher, Mechanical compression release device in steel bracing system for retrofitting RC frames, *Earthq. Eng. Eng. Vib.* 5 (2006) 151–158.
- [8] A. Rahimi, M.R. Maher, The effects of steel X-brace retrofitting of RC frames on the seismic performance of frames and their elements, *Eng. Struct.* 206 (2020), <https://doi.org/10.1016/j.engstruct.2019.110149>.
- [9] A. Rahimi, M.R. Maher, The effects of retrofitting RC frames by X-bracing on the seismic performance of columns, *Eng. Struct.* 173 (2018) 813–830, <https://doi.org/10.1016/j.engstruct.2018.07.003>.
- [10] M.R. Maher, H. Ghaffarzadeh, Connection overstrength in steel-braced RC frames, *Eng. Struct.* 30 (2008) 1938–1948, <https://doi.org/10.1016/j.engstruct.2007.12.016>.
- [11] D. Roke, B. Jeffers, Parametric study of self-centering concentrically-braced frame systems with friction-based energy dissipation, 1st ed. *Behav. STEEL Struct. Seism. Areas* (2012) 691–696.
- [12] M. Dyanati, Q. Huang, D.A. Roke, Structural and nonstructural performance evaluation of self-centering, concentrically braced frames under seismic loading, *Struct. Congr. 2014* (2014) 2393–2404.
- [13] C. Christopoulos, R. Tremblay, H.-J. Kim, M. Lacerte, Self-centering energy dissipative bracing system for the seismic resistance of structures: development and validation, *J. Struct. Eng.* 134 (2008) 96–107, [https://doi.org/10.1061/\(ASCE\)0733-9445\(2008\)134:1\(96\)](https://doi.org/10.1061/(ASCE)0733-9445(2008)134:1(96)).
- [14] D.J. Miller, L.A. Fahnestock, M.R. Eatherton, Development and experimental validation of a nickel-titanium shape memory alloy self-centering buckling-restrained brace, *Eng. Struct.* 40 (2012) 288–298.
- [15] C.-C. Chou, W.-J. Tsai, P.-T. Chung, Development and validation tests of a dual-core self-centering sandwiched buckling-restrained brace (SC-SBRB) for seismic resistance, *Eng. Struct.* 121 (2016) 30–41.
- [16] Y. Zhang, S. Zhu, Seismic response control of building structures with superelastic shape memory alloy wire dampers, *J. Eng. Mech.* 134 (2008) 240–251.

- [17] F. Shi, O.E. Ozbulut, Y. Zhou, Influence of shape memory alloy brace design parameters on seismic performance of self-centering steel frame buildings, *Struct. Control Heal Monit.* 27 (2020) 1–18, <https://doi.org/10.1002/stc.2462>.
- [18] M. Ferraioli, A. Concilio, C. Moliterno, Seismic performance of a reinforced concrete building retrofitted with self-centering shape memory alloy braces, *Procedia Struct. Integr.* 44 (2022) 974–981, <https://doi.org/10.1016/j.prostr.2023.01.126>.
- [19] Dolez M., Cardone D. Theoretical and experimental studies for the application of shape memory alloys in civil engineering 2006.
- [20] R.S. Ingalkar, Rehabilitation of buildings and bridges by using shape memory alloys (SMA), *Int. J. Civ. Eng. Res.* 5 (2014) 163–168.
- [21] Concilio A., Antonucci V., Auricchio F., Lecce L., Sacco E. Shape Memory Alloy Engineering: For Aerospace, Structural, and Biomedical Applications. 2021. (<https://doi.org/10.1016/B978-0-12-819264-1.01001-3>).
- [22] D. Marriott, S. Pampanin, D. Bull, A. Palermo, Dynamic testing of precast, post-tensioned rocking wall systems with alternative dissipating solutions, *Bull. N. Zealand Soc. Earthq. Eng.* 41 (2008) 90–103, <https://doi.org/10.5459/bnzsee.41.2.90-103>.
- [23] A. Wada, Z. Qu, S. Motoyui, H. Sakata, Seismic retrofit of existing SRC frames using rocking walls and steel dampers, *Front. Arch. Civ. Eng. China* 5 (2011) 259–266, <https://doi.org/10.1007/s11709-011-0114-x>.
- [24] N. Makris, M. Aghagholidzadeh, The dynamics of an elastic structure coupled with a rocking wall, *Earthq. Eng. Struct. Dyn.* 46 (2017) 945–962, <https://doi.org/10.1002/eqe.2838>.
- [25] M. Aghagholidzadeh, N. Makris, Seismic response of a yielding structure coupled with a rocking wall, *J. Struct. Eng.* 144 (2018), [https://doi.org/10.1061/\(asce\)st.1943-541x.0001894](https://doi.org/10.1061/(asce)st.1943-541x.0001894).
- [26] M. Ferraioli, B. Laurenza, A. Lavino, C. Frattolillo, G. De Matteis, Seismic retrofit of a steel-reinforced concrete hospital building using continuous energy-dissipative steel columns, *Steel Compos. Struct.* 47 (2023) 467–488, <https://doi.org/10.12989/scs.2023.47.4.467>.
- [27] G. De Matteis, A. Formisano, F.M. Mazzolani, An innovative methodology for seismic retrofitting of existing RC buildings by metal shear panels, *Earthq. Eng. Struct. Dyn.* 38 (2009) 61–78, <https://doi.org/10.1002/eqe.841> (An).
- [28] Z. Yao, W. Wang, Y. Zhu, Experimental evaluation and numerical simulation of low-yield-point steel shear panel dampers, *Eng. Struct.* 245 (2021), 112860, <https://doi.org/10.1016/j.engstruct.2021.112860>.
- [29] M. Ferraioli, A. Lavino, G. De Matteis, A design method for seismic retrofit of reinforced concrete frame buildings using aluminum shear panels, *Arch. Civ. Mech. Eng.* 23 (2023) 1–29, <https://doi.org/10.1007/s43452-023-00639-1>.
- [30] J.D. Marshall, F.A. Charney, Seismic response of steel frame structures with hybrid passive control systems, *Earthq. Eng. Struct. Dyn.* 41 (2012) 715–733.
- [31] C.S. Tsai, K.-C. Chen, C.-S. Chen, Seismic resistibility of high-rise buildings with combined velocity-dependent and velocity-independent devices, *ASME-PUBLICATIONS-PVP* 366 (1998) 103–110.
- [32] J. Lee, J. Kim, Seismic performance evaluation of moment frames with slit-friction hybrid dampers, *Earthq. Struct.* 9 (2015) 1291–1311.
- [33] J. Lee, H. Kang, J. Kim, Seismic performance of steel plate slit-friction hybrid dampers, *J. Constr. Steel Res.* 136 (2017) 128–139.
- [34] M.N. Eldin, J. Kim, J. Kim, Optimum distribution of steel slit-friction hybrid dampers based on life cycle cost, *Steel Compos. Struct.* 27 (2018) 633–646.
- [35] A. Naeem, M.N. Eldin, J. Kim, J. Kim, Seismic performance evaluation of a structure retrofitted using steel slit dampers with shape memory alloy bars, *Int. J. Steel Struct.* 17 (2017) 1627–1638.
- [36] G. Pekcan, J.B. Mander, S.S. Chen, Balancing lateral loads using tendon-based supplemental damping system, *J. Struct. Eng.* 126 (2000) 896–905.
- [37] S. Sorace, G. Terenzi, The damped cable system for seismic protection of frame structures—Part I: General concepts, testing and modeling, *Earthq. Eng. Struct. Dyn.* 41 (2012) 915–928.
- [38] S. Sorace, G. Terenzi, Non-linear dynamic modelling and design procedure of FV spring-dampers for base isolation, *Eng. Struct.* 23 (2001) 1556–1567.
- [39] A. Naeem, J. Kim, Seismic retrofit of a framed structure using damped cable systems, *Steel Compos. Struct.* 29 (2018) 287–299, <https://doi.org/10.12989/scs.2018.29.3.287>.
- [40] A. Naeem, J. Kim, Seismic performance evaluation of a spring viscous damper cable system, *Eng. Struct.* 176 (2018) 455–467.
- [41] AISC. Specification for Structural Steel Buildings, an American National Standard, 2016.
- [42] AIK. KDS 14 31 25:2017, Steel Structure Connection Design Criteria (Load Resistance Factor Design Method), 2017.
- [43] ASTM, Standard test methods and definitions for mechanical testing of steel products, American Society for Testing and Materials, 2017.
- [44] AIK. KDS 41 17 00, Seismic Design Standards for Buildings, Architectural Institute of Korea, 2019.
- [45] ACI Committee. Building Code Requirements for structural concrete (ACI 318-19). American Concrete Institute; 2019.
- [46] J.-Y. Lee, M. Haroon, J. Park, C. Kim, Longitudinal axial strain in plastic hinge regions of reinforced-concrete columns, *Mag. Concr. Res.* 71 (2019), <https://doi.org/10.1680/jmacr.17.00438>.
- [47] M. Haroon, D.I. Shin, J.-Y. Lee, C. Kim, Deformability of reinforced concrete columns failing in shear after flexural reinforcement yielding, *Acids Struct. J.* (2020), <https://doi.org/10.14359/51721377>.
- [48] Grondin G., Jin M., Josi G. Slip Critical Bolted Connections — A Reliability Analysis for Design at the Ultimate Limit State. vol. 76. 2008.